A Single-Channel Algorithm for Land-Surface Temperature Retrieval From ASTER Data

Juan C. Jiménez-Muñoz and José A. Sobrino

***Abstract*—This letter presents an adaptation to Advanced Spaceborne Thermal Emission and Reflection Radiometer (ASTER) data of the generalized single-channel (SC) algorithm developed by Jiménez-Muñoz and Sobrino, also adapted to the Landsat thermal-infrared (TIR) channel (band 6) later by Jiménez-Muñoz *et al.* The SC algorithm relies on the concept of atmospheric functions (AFs), which are dependent on atmospheric transmissivity, upwelling, and downwelling atmospheric radiances. These AFs are fitted versus the atmospheric water–vapor content for operational purposes, despite the fact that other computation options are also possible. The SC algorithm has been adapted to ASTER TIR bands 13 (10.659 μm) and 14 (11.289 μm), located in the typical split-window region (10.5–12 μm), where transmission through the atmosphere is higher and surface emissivity variations are lower in comparison with the ones in the 8–9.4 μm spectral region. Land-surface temperature retrieved with the SC algorithm has been tested over five different samples (including vegetated plots and bare soil) in an agricultural area using one single image. The comparison with ground-truth data provided a bias near to zero and standard deviations of around 2 K, with bands 13 and 14 providing similar results.**

***Index Terms*—Advanced Spaceborne Thermal Emission and Reflection Radiometer (ASTER), land-surface temperature (LST), single-channel (SC), thermal infrared (TIR).**

I. Introduction

THE ADVANCED Spaceborne Thermal Emission and Reflection Radiometer (ASTER) on the National Aeronautics and Space Administration's Terra platform is the highest spatial resolution (90 m) multispectral thermal-infrared (TIR) imaging sensor currently available on a polar-orbiting spacecraft. The ASTER science team provides standard products of both land-surface temperature (LST) and surface emissivities (AST-08 and AST-05, respectively), retrieved with the temperature and emissivity separation (TES) algorithm [1], which are available through the Eros Data Center [2]. TES products were validated and found to perform within specification of ± 0.015 for emissivity and ± 1.5 K for LST. However, some inaccuracies have been found over low spectral-contrast surfaces, as is the case with agricultural areas. These problems were expected and pointed out in [1] and have been explicitly analyzed over agricultural areas in [3] and [4]. Some modifications to the TES processing chain have been proposed to partially avoid those problems [5].

An alternative procedure to retrieve LST from ASTER data was assessed in [6] by using split-window (SW) algorithms, where input emissivities can be computed from the normalized difference vegetation index (NDVI) [3]. Results from simulated and ground-truth data provided similar errors to those ones specified for TES products, although ASTER TIR bands are not specially designed to work with such SW algorithms, and uncertainties on LST retrievals are significantly sensitive to uncertainties on input parameters (mainly, surface emissivities and noise-equivalent delta temperatures).

This letter is oriented to scientific users interested on LST retrieval: 1) but they are not familiar with TES implementation, 2) they have no access to the LST TES standard product AST-08, or 3) they have found inaccuracies in that standard product and want to retrieve LST with an alternative method, which is not the SW algorithm mentioned in the previous paragraph. For this purpose, we present a single-channel (SC) algorithm that is easy to implement, which is based on the algorithm developed by Jiménez-Muñoz and Sobrino (JM&S) [7], and it has been adapted to ASTER data following the procedure adopted for Landsat TIR data [8]. For more details, the reader is referred to those references. In this letter, we will provide the particular expressions needed to retrieve LST using the proposed SC, hereinafter denoted as $\mathrm{SC}^{\mathrm{JM\&S}}$.

II. SC Algorithm

A. Theory

The $\mathrm{SC}^{\mathrm{JM\&S}}$ algorithm retrieves LST (T_s) using the following general equation:

$$T_s = \gamma \left[\frac{1}{\varepsilon}(\psi_1 L_{sen} + \psi_2) + \psi_3 \right] + \delta \tag{1}$$

where ε is the surface emissivity, γ and δ are two parameters dependent on the Planck's function, and ψ_1, ψ_2, and ψ_3 are referred to as atmospheric functions (AFs) and given by

$$\psi_1 = \frac{1}{\tau} \quad \psi_2 = -L^{\downarrow} - \frac{L^{\uparrow}}{\tau} \quad \psi_3 = L^{\downarrow} \tag{2}$$

where τ is the atmospheric transmissivity, $L^{\uparrow}$ is the upwelling atmospheric radiance, and $L^{\downarrow}$ is the downwelling atmospheric radiance. All the previous magnitudes are spectral,

Manuscript received June 12, 2009. First published September 22, 2009; current version published January 13, 2010. This work was supported in part by the European Space Agency (SPARC, Project RFQ/3-10824/03/NL/FF), by the European Union (CEOP-AEGIS, Project FP7-ENV-2007-1 Proposal 212921; WATCH, Project 036946), and by the Ministerio de Ciencia y Tecnología (EODIX, Project AYA2008-0595-C04-01).

The authors are with the Global Change Unit, Image Processing Laboratory, University of Valencia, 46071 Valencia, Spain (e-mail: jcjm@uv.es; sobrino@uv.es).

Color versions of one or more of the figures in this paper are available online at http://ieeexplore.ieee.org.

Digital Object Identifier 10.1109/LGRS.2009.2029534

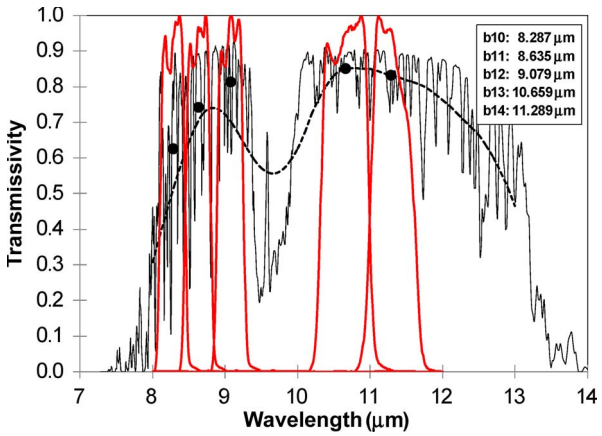

Fig. 1. Spectral-response functions for the five ASTER thermal bands, overlapped to a transmissivity spectrum for a midlatitude summer atmosphere. Dashed line corresponds to the smoothed spectrum (with a bandpass of 1 μm), whereas black points show the effective transmissivity values for ASTER bands.

i.e., dependent on the wavelength λ, but spectral notation will be omitted for simplicity.

B. ASTER Thermal Bands

The SC$^{\mathrm{JM\&S}}$ algorithm is applied only to one TIR band. Since ASTER has five different TIR bands, the optimal band should be selected in order to apply the algorithm, although it could be applied to any ASTER TIR band and, in fact, to any thermal band of any sensor. It is expected that LST retrievals are more accurate in the typical SW region between 10 and 12 μm, where atmospheric transmission is higher and emissivity variations are lower in comparison with other atmospheric windows, such as the one between 8 and 9 μm. Fig. 1 shows an example of atmospheric transmissivity for a midlatitude summer atmosphere, in which a smoothed spectrum ASTER TIR spectral response functions and effective transmissivity values for those TIR bands are overlapped. Bands 12, 13, and 14 show the highest atmospheric transmissivity. Since band 12 is located around 9 μm, bands 13 and 14 are the optimal ones for LST retrieval with the SC algorithm.

C. Gamma and Delta Parameters

When working with TIR data, it is common to convert at-sensor registered radiances (L_{sen}) into at-sensor brightness temperatures (T_{sen}). Although L_{sen} appears explicitly in (1), T_{sen} is also needed to compute the γ and δ parameters, as will be shown next. We will compute T_{sen} using inversion of the Planck's law and the concept of effective wavelength, i.e.,

$$T_{\mathrm{sen}} = \frac{K_2}{\ln\left(\frac{K_1}{L_{\mathrm{sen}}} + 1\right)} \tag{3}$$

where $K_2 = c_2/\lambda$ and $K_1 = c_1/\lambda^5$, with c_1 and c_2 as the radiation constants, and λ is the effective wavelength. Fig. 1 shows values of effective λ, whereas values of K_1 and K_2 are provided in Table I.

TABLE I
RADIATION CONSTANTS USED IN (3)

ASTER band	K_1 [W·m^{-2}·sr^{-1}·μm^{-1}]	K_2 [K]
10	3047.47	1736.18
11	2480.93	1666.21
12	1930.80	1584.72
13	865.65	1349.82
14	649.60	1274.49

Parameters γ and δ, involved in (1), can be computed from the following approximation [8]:

$$\gamma \approx \frac{T_{\mathrm{sen}}^2}{K_2 L_{\mathrm{sen}}}$$
$$\delta \approx T_{\mathrm{sen}} - \frac{T_{\mathrm{sen}}^2}{K_2} \tag{4}$$

where T_{sen} is computed from (3) and K_2 values are given in Table I.

III. AFs

The AFs given by (2) can be computed from different ways:

1) directly from τ, $L^{\uparrow}$ and $L^{\downarrow}$ values, which can be obtained from atmospheric soundings and radiative transfer codes such as MODTRAN4 [9];
2) using empirical approaches with only one input parameter such as the total atmospheric water-vapor content [7], [8];
3) using empirical approaches with two input parameters, such as water vapor and air temperature [10];
4) from lookup tables [8].

Despite the fact that option 1) is *a priori* the optimal one, the SC$^{\mathrm{JM\&S}}$ was originally developed with the purpose of using minimal and more accessible input data; therefore, we will focus, in this letter, with option 2).

AFs can be empirically obtained from second-order polynomial fits versus the atmospheric water-vapor content [7], [8]

$$\begin{bmatrix} \psi_1 \\ \psi_2 \\ \psi_3 \end{bmatrix} = \begin{bmatrix} c_{11} & c_{12} & c_{13} \\ c_{21} & c_{22} & c_{23} \\ c_{31} & c_{32} & c_{33} \end{bmatrix} \begin{bmatrix} w^2 \\ w \\ 1 \end{bmatrix} \tag{5}$$

where coefficients c_{ij} are obtained from simulated data constructed from atmospheric profiles included in different databases and MODTRAN4 radiative transfer code. Five different atmospheric-profile databases were used in [8]. In this letter, we focus on TIGR61 and STD66 databases as described in [8]. These databases have a reduced number of atmospheric cases, thus reducing computing time on the simulation but are suitable for global conditions. Table II shows the coefficients obtained for these two databases and for ASTER TIR bands 13 and 14. Since ASTER's field of view is 8°, simulations were performed only for nadir view angles.

IV. VALIDATION

The LST retrievals from the SC algorithm proposed in this letter were tested against *in situ* measurements collected over

TABLE II
COEFFICIENTS FOR THE ATMOSPHERIC FUNCTIONS FOLLOWING MATRIX NOTATION IN (5). VALUES HAVE BEEN OBTAINED USING DIFFERENT ATMOSPHERIC SOUNDING DATABASES FOR ASTER BANDS 13 AND 14

Database	Band	Cij	i=1	i=2	i=3
STD66	13	j=1	0.06524	-0.05878	1.06576
		j=2	-0.55835	-0.75881	0.00327
		j=3	-0.00284	1.35633	-0.43020
TIGR61	13	j=1	0.05327	-0.03937	1.05742
		j=2	-0.48444	-0.74611	-0.03015
		j=3	0.00764	1.24532	-0.39461
STD66	14	j=1	0.10062	-0.13563	1.10559
		j=2	-0.79740	-0.39414	-0.17664
		j=3	-0.03091	1.60094	-0.56515
TIGR61	14	j=1	0.07965	-0.09580	1.08983
		j=2	-0.66528	-0.48582	-0.17029
		j=3	-0.01578	1.46358	-0.52486

five different plots (green grass, alfalfa, bare soil, and two plots of corn) in an agricultural area in Spain (Barrax, 39° 3′ N, 2° 6′ W, 700 m), and using a single ASTER image acquired on July 18, 2004. A detailed description of the ASTER data and measurement procedure can be found in [4].

Four different LST retrieval procedures from the SC technique were considered:

1) Radiative transfer equation (RTE): direct inversion of RTE using the local atmospheric sounding and MODTRAN to compute the atmospheric parameters τ, $L^{\uparrow}$, and $L^{\downarrow}$;
2) SOUND: the SC$^{\mathrm{JM\&S}}$ algorithm, as described in this letter, where the AFs are computed directly from (2) and the parameters τ, $L^{\uparrow}$, and $L^{\downarrow}$, as in case 1);
3) STD66: the SC$^{\mathrm{JM\&S}}$ algorithm, as described in this letter, where AFs are computed from empirical approaches [(5)] using coefficients obtained from STD66 database (Table II);
4) TIGR61: same as case 3) but using TIGR61 database.

In cases 3) and 4), a w value of 1.74 g/cm^2 was considered, which was extracted from the local atmospheric sounding launched near the overpass time of ASTER.

In all cases, surface emissivity was retrieved using the NDVI approach [3]. Results are provided in Table III for ASTER band 13 and Table IV for ASTER band 14. It is observed that ASTER band 13 provides slightly better results than band 14, with rmse values below 2 K. Results obtained for cases 1) and 2) are slightly better than the ones obtained for cases 3) and 4), as is expected, but the improvements in the first two cases are minimal thus showing that empirical approaches with water vapor are also suitable for the LST retrieval. The rmse differences between STD66 and TIGR61 are below 0.2 K thus providing similar results. The highest differences were obtained for the bare-soil plot, with values near to 3 K for band 13 and around 4 K for band 14. These large differences can be attributed to the problem of the different scale between the ASTER and *in situ* measurements, jointly with the turbulence-induced temperature fluctuations, as discussed in [4]. When the bare-soil plot is not considered in the test, rmse values are below 1.5 K for band 13 and below 1.2 K for band 12, thus, band 14 provides slightly better results in this case. Fig. 2 shows an example of the LST map obtained with the SC algorithm applied to band 13.

TABLE III
DIFFERENCE (Δ) BETWEEN LAND-SURFACE TEMPERATURES RETRIEVED WITH THE SC ALGORITHM APPLIED TO ASTER BAND 13 AND THE ONES MEASURED *IN SITU* ($T_{in\ situ}$, WITH STANDARD DEVIATION IN BRACKETS). TEST PLOTS ARE BARE SOIL (BS), GREEN GRASS (GG), ALFALFA (A) AND TWO CORN PLOTS (C1 AND C2). BIAS, STD, AND RMSE VALUES OBTAINED WHEN BS PLOT IS NOT CONSIDERED ARE GIVEN IN BRACKETS

Plot	$T_{\text{in-situ}}$ (K)	Δ_{RTE} (K)	Δ_{SOUND} (K)	Δ_{STD66} (K)	Δ_{TIGR61} (K)
BS	326.8 (1.2)	-2.82	-2.6	-2.57	-3.4
GG	311.2 (1.5)	0.6	0.8	1.3	1.2
A	300.1 (1.2)	1.4	1.5	2.4	2.3
C1	303 (2)	-1.1	-1	-0.1	-0.2
C2	301.7 (1.7)	-0.52	-0.5	0.45	0.35
	BIAS	-0.5 (0.1)	-0.4 (0.2)	0.3 (1.0)	0.0 (0.9)
	STD	1.6 (1.1)	1.6 (1.2)	1.9 (1.1)	2.1 (1.1)
	RMSE	1.7 (1.1)	1.6 (1.2)	1.9 (1.5)	2.1 (1.4)

TABLE IV
SAME AS TABLE III, BUT FOR ASTER BAND 14

Plot	$T_{\text{in-situ}}$ (K)	Δ_{RTE} (K)	Δ_{SOUND} (K)	Δ_{STD66} (K)	Δ_{TIGR61} (K)
BS	326.8 (1.2)	-4.08	-3.8	-4.1	-4.2
GG	311.2 (1.5)	0.1	0.2	0.7	0.7
A	300.1 (1.2)	1	1	2.1	2.1
C1	303 (2)	-1.38	-1.37	-0.27	-0.25
C2	301.7 (1.7)	-0.7	-0.7	0.4	0.4
	BIAS	-1.0 (-0.2)	-0.9 (-0.2)	-0.2 (0.7)	-0.3 (0.7)
	STD	1.9 (1.0)	1.8 (1.0)	2.3 (1.0)	2.4 (1.0)
	RMSE	2.2 (1.1)	2.1 (1.1)	2.3 (1.2)	2.4 (1.2)

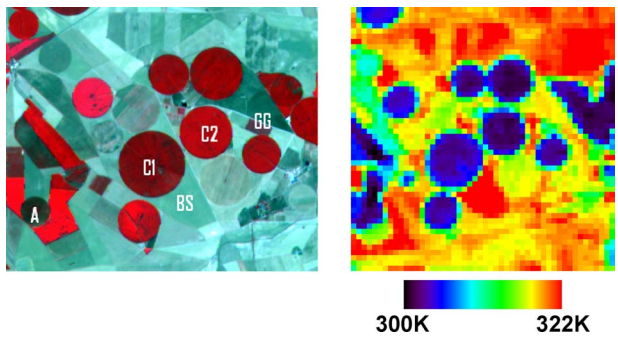

Fig. 2. Example of LST map retrieved with the SC algorithm applied to ASTER band 13 using TIGR61 coefficients. On the right, an RGB composition (bands 3, 2, 1) with validation plots marked and on the left, the LST map. Geographic coordinates for image center are 39° 3′ 33.10″ N and 2° 6′ 5.23″ W.

V. DISCUSSION AND CONCLUSION

TES algorithm [1] is preferred to retrieve LST and emissivity from ASTER data, since it makes use of the ASTER

multispectral TIR characteristics, and it provides emissivity estimations in a pixel-by-pixel basis by solving the RTE. For this reason, TES emissivities are indicative of land-cover changes, contrary to emissivities retrieved from NDVI approaches, which do not respond to changes in vegetation-canopy densities and to changes in the surface-soil properties [11]. However, NDVI approaches provide better quality emissivity maps than TES over agricultural areas, where surfaces have low spectral contrast and pixels are composed by a mixture of soil and vegetation. These approaches are also easy to apply for nonexperienced users, and they can be used as input to other simple LST-retrieval algorithms such as SW or SC ones. In this letter, we have presented an SC algorithm that can be applied to any ASTER TIR band but preferably to ASTER band 13 or 14. Comparison with ground-truth data provided errors below 2 K when using band 13, although validations were performed using only one single image but five different plots. Despite being slightly worse, errors are on the same order with the ones obtained with the SW algorithms [6] and TES standard product [4] over the same area. Therefore, and despite that, we encourage the use of the TES algorithm; the user has an alternative to estimate surface emissivity using the NDVI approach [3] and at least two alternatives to retrieve LST from ASTER data: 1) the SW technique [6] and 2) the SC algorithm presented in this letter. Note that the SW and SC algorithms can be applied to other surfaces other than agricultural ones, such as water, rocks, or even urban areas, but in these cases, input emissivities should be estimated from different approaches other than the NDVI ones.

ACKNOWLEDGMENT

The authors would like to thank A. Gillespie, D. Sabol, and W. T. Gustafson (University of Washington) for their helpful scientific and technical support.

REFERENCES

[1] A. Gillespie, S. Rokugawa, T. Matsunaga, J. S. Cothern, S. Hook, and A. B. Kahle, "A temperature and emissivity separation algorithm for Advanced Spaceborne Thermal Emission and Reflection Radiometer (ASTER) images," *IEEE Trans. Geosci. Remote Sens.*, vol. 36, no. 4, pp. 1113–1126, Jul. 1998.

[2] M. Abrams, "The Advanced Spaceborne Thermal Emission and Reflection Radiometer (ASTER): Data products for the high spatial resolution imager on NASA's terra platform," *Int. J. Remote Sens.*, vol. 21, no. 5, pp. 847–859, Mar. 2000.

[3] J. C. Jiménez-Muñoz, J. A. Sobrino, A. Gillespie, D. Sabol, and W. T. Gustafson, "Improved land surface emissivities over agricultural areas using ASTER NDVI," *Remote Sens. Environ.*, vol. 103, no. 4, pp. 474–487, Aug. 2006.

[4] J. A. Sobrino, J. C. Jiménez-Muñoz, L. Balick, A. Gillespie, D. Sabol, and W. T. Gustafson, "Accuracy of ASTER level-2 thermal-infrared standard products of an agricultural area in Spain," *Remote Sens. Environ.*, vol. 106, no. 2, pp. 146–153, Jan. 2007.

[5] W. T. Gustafson, A. R. Gillespie, and G. J. Yamada, "Revisions to the ASTER temperature/emissivity separation algorithm," in *Proc. Recent Adv. Quantitative Remote Sens.*, Valencia, Spain, Sep. 25–29, 2006, pp. 770–775.

[6] J. C. Jiménez-Muñoz and J. A. Sobrino, "Feasibility of retrieving land-surface temperature from ASTER TIR bands using two-channel algorithms: A case study of agricultural areas," *IEEE Geosci. Remote Sens. Lett.*, vol. 4, no. 1, pp. 60–64, Jan. 2007.

[7] J. C. Jiménez-Muñoz and J. A. Sobrino, "A generalized single-channel method for retrieving land surface temperature from remote sensing data," *J. Geophys. Res.*, vol. 108, no. D22, p. 4688, Nov. 2003, DOI:10.1029/2003JD003480.

[8] J. C. Jiménez-Muñoz, J. Cristóbal, J. A. Sobrino, G. Sòria, M. Ninyerola, and X. Pons, "Revision of the single-channel algorithm for land surface temperature retrieval from Landsat thermal-infrared data," *IEEE Trans. Geosci. Remote Sens.*, vol. 47, no. 1, pp. 339–349, Jan. 2009.

[9] A. Beck, G. P. Anderson, P. K. Acharya, J. H. Chetwynd, L. S. Bernstein, E. P. Shettle, M. W. Matthew, and S. M. Adler-Golden, *MODTRAN4 User's Manual*. Hanscom AFB, MA: Air Force Res. Lab., 1999.

[10] J. Cristóbal, J. C. Jiménez-Muñoz, J. A. Sobrino, M. Ninyerola, and X. Pons, "Improvements in land surface temperature retrieval from the Landsat series thermal band using water vapor and air temperature," *J. Geophys. Res.*, vol. 114, p. D08 103, Apr. 2009, DOI:10.1029/2008JD010616.

[11] A. N. French, T. J. Schmugge, J. C. Ritchie, A. Hsu, F. Jacob, and K. Ogawa, "Detecting land cover change at the Jornada experimental range, New Mexico with ASTER emissivities," *Remote Sens. Environ.*, vol. 112, no. 4, pp. 1730–1748, Apr. 2008.